Revista de Chimie
https://revistadechimie.ro
https://doi.org/10.37358/Rev.Chim.1949

Considerable Improvement in Fenton-like Degradation of MB Owing to Ti^{3+}/Ti^{4+} Using Ion-doped Halloysite Nanotube Catalyst

YUAN WEI[1], YATING SUN[1], DAHUA LI[2], BINDA LU[1], MIAOHUA LIU[3], GONGGANG LIU[1*], JINBO HU[1*]

[1]Central South University of Forestry and Technology, Hunan Province Key Laboratory of Materials Surface & Interface Science and Technology, College of Materials Science and Engineering, Shaoshan South Road, No. 498, Changsha 410004, China

[2]Fudan University, The Key Laboratory of Molecular Engineering of Polymers and Department of Macromolecular Science, Shanghai 200433, China

[3]Central South University, School of Minerals Processing and Bioengineering, Lushan South Road, No. 932, Changsha 410006, China

Abstract: *Due to high efficiency and environmental friendship, Fenton-like technology is widely used in water treatment and has always received significant attentions, especially in design of novel and efficient Fenton-like catalysts. In this paper, iron/titanium ions doped halloysite nanotubes (HNTs-Fe-Ti) have been developed as Fenton-like catalyst. Here, halloysite nanotubes (HNTs) with high specific surface area and excellent ion exchange capacity were used as carriers, and iron/titanium ions were trace-doped into HNTs via simple ion-exchange reaction. The degradation of the designed catalyst for methylene blue (MB) was greatly accelerated in the presence of titanium ion. It demonstrates that the excellent degradation ability mainly owes to the valence state transformation of titanium and the good adsorption ability of halloysite nanotubes. It shows the mechanism of titanium with multivalent states (Ti^{3+}/Ti^{4+}) on the degradation of MB is similar to the Fenton catalytic mechanism of iron ion transformation (Fe^{2+}/Fe^{3+}). In the Fenton-like degradation reaction, titanium and iron play a synergistic catalytic role in MB degradation while titanium has greater impact. When the ratio of titanium to iron is 5:1, the catalyst exhibits superior Fenton-like degradation performance, and the degradation rate could reach 91% at 100 min.*

Keywords*: halloysite nanotubes, Ti, Fe, Fenton-like, methylene blue, water treatment*

1. Introduction

Dye-printing wastewater contains a variety of dyes which are difficult to degrade [1, 2]. Widespread organic pollutions from dyes have drawn great concerns of health-environment. And lots of methods are utilized to treat dye waste water. At present, the treatment technologies mainly include biodegradation, physical adsorption, membrane separation, coagulation precipitation and advanced oxidation technology [3–7]. Advanced oxidation processes (AOPs) have been one of great potential technologies for the removal of organic dyes from wastewater due to strong oxidizing/mineralizing ability, environmental friendship, good applicability and high efficiency [8]. AOPs are characterized by the generation of much and highly oxidative hydroxyl radicals (•OH) in solution. •OH is able to destroy the most organics until their complete mineralization into CO_2, water, and inorganic ions [9, 10]. AOPs include plasma oxidation, wet air oxidation, Fenton reaction, the use of ultrasound/microwaves/γ-irradiation/electrochemical processes, and so on [11, 12]. And Fenton reaction based on Fe^{2+} and H_2O_2 is widely used in dye-printing wastewater treatment due to its advantages of strong oxidation and fast reaction rate [13, 14]. However, it constrains its commercial application resulting from narrow *p*H, sludge production during operation and constant *p*H adjustment process [15, 16].

**email: liugonggang@csuft.edu.cn, hjb1999@hotmail.com*

Fenton-like reaction, which mainly utilize iron based materials in the form of powder, such as Fe_2O_3 [17, 18], Fe_3O_4 [19, 20], iron oxyhydroxide [21, 22], nanoscale zero-valent iron [23, 24], has been developed to avoid the mentioned problems from Fenton reaction, especially for the supported heterogeneous catalyst. The supported heterogeneous catalyst can be easily recovered and reused, and extend the range of *p*H in presence of carrier. Besides, porous carrier with a high specific surface area could improve the catalytic degradation ability of Fenton-like reaction with outstanding adsorption performance for the pollutants [5]. In addition to Fe-based catalysts, other transition metal ions, such as Cu [25], Co [26], Mn [27], Ni [28], Cr [29], are also used as Fenton-like catalysts and show decent catalytic performance. However, some of these transition metal ions have some toxicity [30], and the ion leaching may result in secondary water pollution. On the other hand, the catalytic activity of Fenton-like catalyst should be further improved to facilitate their industrial process compared with high-efficient Fenton reaction. Hence the development of higher efficient and more eco-friendly Fenton-like catalyst is still a great challenge.

Titanium is a transition metal with low toxicity, and titanium dioxide is widely used as an environmentally friendly photocatalyst in the field of photocatalysis because of its non-toxic and harmless, high photocatalytic activity and stability [31–33]. For titanium ions with multivalent states, the valence state transformation exists [34]. Similar to the catalytic mechanism of other transition metal ions based Fenton-like reaction, titanium based material is a nice choice for Fenton-like catalyst.

In this work, titanium-iron ion doped halloysite nanotubes (HNTs) have been developed as Fenton-like catalyst (HNTs-Fe-Ti). HNTs with high-specific surface area and excellent ion exchange capacity were used as carriers, and iron/titanium ions were trace-doped into HNTs via simple ion-exchange reaction. The prepared materials were characterized by TEM, SEM, EPR, BET and XPS. Moreover the Fenton-like catalytic performances of the prepared catalysts were studied in detail. Besides, the catalytic mechanism of the prepared catalyst for Fenton-like reaction was also discussed. This study designed a new type of catalyst and discovered the role of Ti^{3+}/Ti^{4+} valence state conversion mechanism in the catalytic degradation process for prominently enhanced catalytic ability. It will provide new ideas for the development of high-efficiency and more eco-friendly Fenton-like catalysts.

2. Materials and methods

2.1. Chemicals and materials

The Halloysite nanotubes (HNTs) were purchased from Zhengzhou Jinyangguang Chinaware Co., Ltd. Titanium oxysulfate (IV) ($TiOSO_4$), ferric trichloride ($FeCl_3$), potassium borohydride (KBH_4), methylene blue (MB), hydrogen peroxide aqueous solution (H_2O_2, 30%) were purchased from Sigma-Aldrich and used directly.

2.2. Preparation of catalysts

Typically, 4.0 g $TiOSO_4$ and 1.0 g $FeCl_3$ were added into 20 mL H_2O, and stirred thoroughly to form a transparent and clear solution (*p*H=1). Then 0.5 g HNTs were added into the solution, then mixed thoroughly and stirred for 12 h. After filtration, the sample was washed with deionized water several times. After that 0.2 g KBH_4 into 20 mL H_2O was added into the residue, and stirred for 2 h. Here, KBH_4 was used to reduce Ti^{4+} and Fe^{3+} to Ti^{3+} and Fe^0, respectively. Then it was filtered, washed and dried to obtain HNTs-Fe-Ti (the molar ratio of Fe to Ti is 1:5).

In order to evaluate the effect of Fe/Ti ratio on the catalytic degradation performance, the catalysts loaded with different ratios of Fe/Ti were prepared. The molar ratios of Fe to Ti were 1:0, 1:10, 1:1, 2:1 and 0:1, respectively. Meanwhile, HNTs-Fe-Ti and HNTs-Ti without KBH_4 treatment were prepared as control samples. In order to further verify the Fenton-like catalytic mechanism of HNTs-Fe-Ti catalysts, the catalytic efficiency of $TiOSO_4$ and P25 reduced by KBH_4 for MB was also evaluated. Here, the preparation of the HNTs-Fe-Ti catalyst and their Fenton-like reaction process were presented in Figure 1.

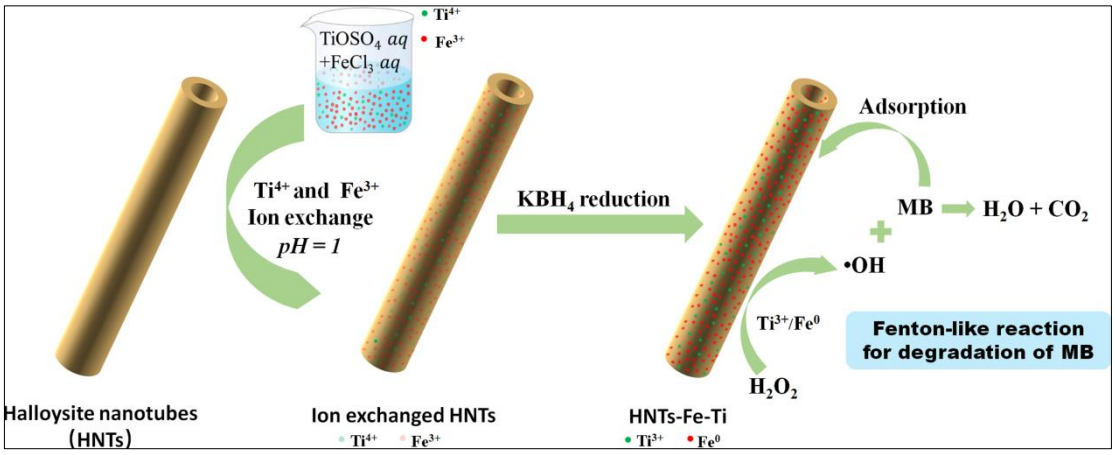

Figure 1. Preparation of the HNTs-Fe-Ti catalyst and their Fenton-like process

2.3. Characterization

The morphologies of the samples were characterized by scanning electron microscopy (FE-SEM, Tesca MIRA3) and transmission electron microscopy (TEM, HT7800). The pore structure and specific surface area were measured at 77.3 K with Quantachrome NOVA 2200e instrument. The 752N UV-Vis spectrophotometer with a detection wavelength at 664 nm was used to analyze MB solution. X-ray photoelectron spectra of the catalysts were recorded using X-ray photoelectron spectrometer (XPS, Thermo Scientific K-Alpha+) with aluminium (mono) K_α source (72 W). Electron paramagnetic resonance (EPR) spectrometer was used to detect the existence of hydroxyl radical (•OH) in Fenton-like reaction. The detection was under dark conditions, then 50 mg of the prepared HNTs-Fe-Ti catalyst, 20 mL of deionized water and 1 mL of 30% H_2O_2 solution were mixed for 5 min. Next, 100 µL of the mixture was took out and injected into 50 µL of DMPO to detect. Here, DMPO was used as free radical scavenger, and the DMPO-OH adducts were tested by EPR spectrometer (Bruker A300).

2.4. Catalytic performance

The catalytic degradation experiment was carried out at completely dark condition to avoid the influence of light on the decomposition of H_2O_2 and the degradation of organic. The target pollutant was prepared with 0.2 L MB solution (10 mg·L^{-1}). Then 0.613 mL of 30% H_2O_2 solution and 0.05 g of the prepared catalyst were added, and fully stirred to react. Next, the reaction mixture was taken out every 5 min, centrifuged and settled. The absorbance value of supernatant was measured at the maximum absorption wavelength (664 nm) by visible spectrophotometer. The absorbance value versus reaction time (C/C_0 versus t) were obtained, which reflected the decrease of the MB concentration, and the MB decolorization efficiency was calculated as follows (Equation 1):

$$\text{Decolorization efficiency (\%)} = 100\times(C_0-C)/C_0 \quad (1)$$

where C_0 is the initial MB concentration and C is the MB concentration. Besides, in order to better explore the catalytic mechanism, the adsorption ability of different catalysts was tested.

3. Results and discussions

3.1. Characterization of samples

The morphology and size of the HNTs and HNTs-Fe-Ti samples are observed by SEM and TEM characterization. Figure 2 shows the SEM images and corresponding elemental mapping of HNTs (a~d) and HNTs-Fe-Ti (e~h). As can be seen from the SEM images of HNTs (Figure 2a) and HNTs-Fe-Ti (Figure 2e), HNTs have a short rod-like structure with a relatively uniform size, and it has no significant difference with HNTs-Fe-Ti. The results of the O, Ti and Fe elemental mappings of HNTs (Figure 2b-d) and HNTs-Fe-Ti (Figure 2f-h) confirm the presence of element Ti and Fe before and after ions

exchange, and they are uniformly distributed. Unsurprisingly, as HNTs are a kind of silicate clay minerals, they contain small amounts of Ti and Fe elements which could account for the Ti and Fe elemental mappings of HNTs. On the other hand, the EDS results from SEM show the mass percentage of Fe increases from 0.5 to 2% while Ti increases from 0.3% to 1.2%. It's obvious the content of element Ti and Fe increase significantly after Ti and Fe doping. The results show Ti and Fe ions are doped in HNTs successfully via ions exchange.

Further observation is carried out by TEM. From TEM images (Figure 3a, b), it shows that HNTs have a typical ringent tubular structure with a diameter of 40-90 nm and length of 0.5-1.5 μm. Besides, abundant microporous structures could be observed on the wall surfaces of HNTs. For HNTs-Fe-Ti (Figure 3c, d), there is no significant difference with the structure of HNTs. Obviously, no nanoparticles are loaded on the surfaces of HNTs. It indicates that Ti and Fe ions doped HNTs-Fe-Ti catalysts can be considered as the displacement doping via ion exchange method instead of nanoparticles loading. As a consequence of excellent ion exchange capacity of HNTs [35, 36], it is not difficult to explain it.

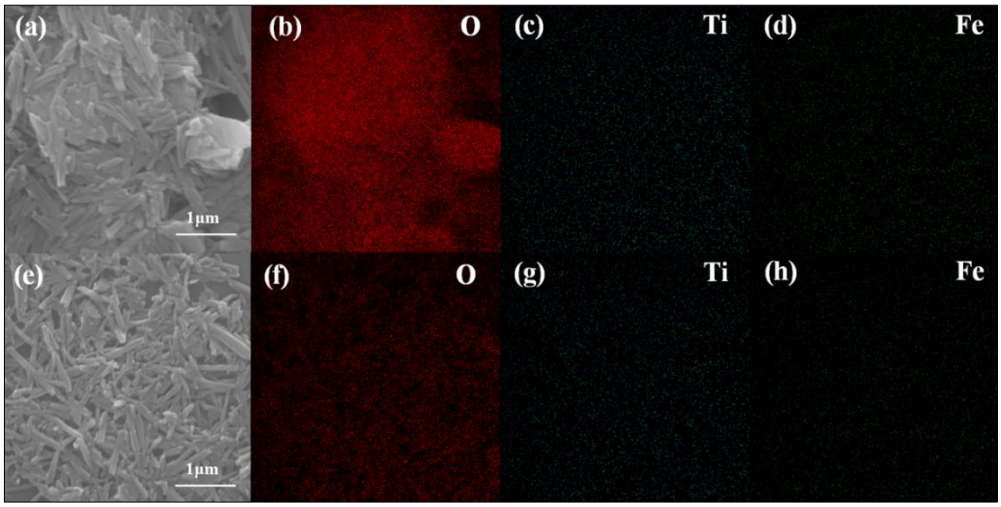

Figure 2. SEM images of (a) HNTs and (e) HNTs-Fe-Ti, and O, Ti, Fe elemental mapping of (b~d) HNTs and (f~h) HNTs-Fe-Ti

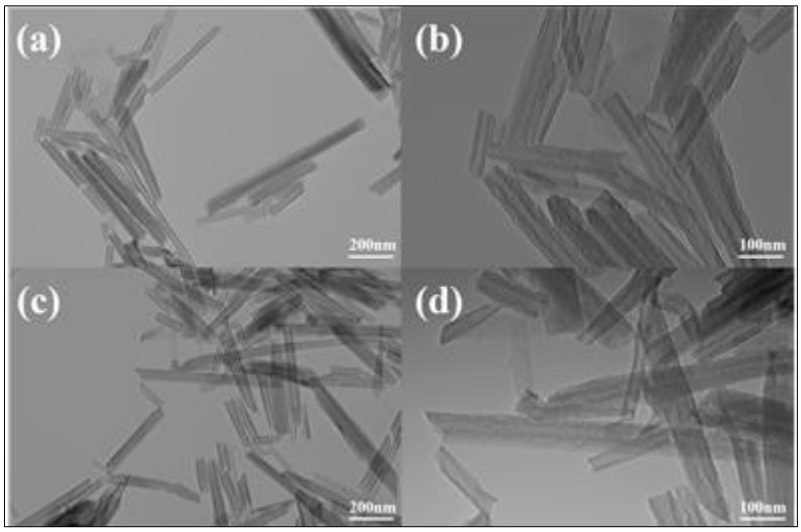

Figure 3. TEM images of (a, b) HNTs and (c, d) HNTs-Fe-Ti

Nitrogen adsorption-desorption isotherm curves of HNTs and HNTs-Fe-Ti at 77 K are shown in Figure 4a. Both the isotherms exhibit similar patterns which belong to type IV with H3 hysteresis loops according to the basis of IUPAC recommendations [37]. It further indicates that the prepared HNTs-Fe-

Ti retains a tubular morphology from the hollow space of HNTs without pore blocking. In addition, calculated from the isotherms using the BET method, the specific surface area of HNTs and HNTs-Fe-Ti are 34.88 $m^2 \cdot g^{-1}$ and 42.39 $m^2 \cdot g^{-1}$, respectively. The specific surface area of HNTs-Fe-Ti was slightly higher than HNTs, it may be because some pores are formed during ion exchange with an acidic condition. And the pore sizes distributions of porous HNTs and HNTs-Fe-Ti are calculated with BJH method as shown in Figure 4b. It indicates that the pore sizes are widely distributed mainly focusing on 3.9 nm and 14.4 nm which attributes to the pores from wall and inner space of HNTs, respectively.

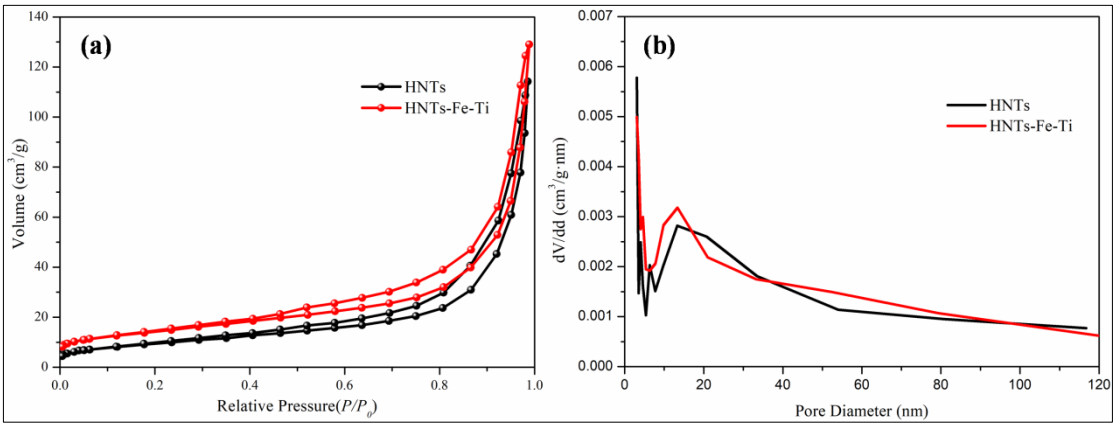

Figure 4. (a) The nitrogen adsorption-desorption isotherms and (b) pore diameter distributions of HNTs and HNTs-Fe-Ti

3.2. Degradation ability of catalysts

In order to study the Fenton-like catalytic abilities of the prepared catalysts, the catalytic degradation performance of different catalysts (HNTs-Fe-Ti, HNTs-Ti, HNTs-Fe and HNTs) was evaluated. The decolorization kinetic curves of MB under different systems are presented in Figure 5. It shows the degradation performance of different types of catalysts (Figure 5a), and the experimental data is averaged by three parallel experiments. The results show that HNTs-Fe-Ti (the ration of Fe to Ti is 1:5) has the highest Fenton-like degradation capacity, the MB decolorization rate was 91% after 100 min. For comparison, HNTs-Ti catalyst (without Fe doping) has a higher Fenton-like catalytic activity for degradation of MB than HNTs-Fe catalyst (without Ti doping), and the MB decolorization rates are 83% and 68% after 100 min, respectively. However, the MB decolorization rate of HNTs is only 53%. The results indicate that titanium ion plays a very important role in enhancing the Fenton-like degradation performance of the catalyst, even surpassing Fe. Besides, Ti and Fe doping have a positive synergistic catalytic effect in the degradation of MB.

The effect of adsorption capacity of the catalysts on Fenton-like reaction was further studied, and the adsorption performances of different types of catalysts (HNTs-Fe-Ti, HNTs-Ti, HNTs-Fe and HNTs) for MB are shown in Figure 5b. The result shows that both of them have excellent the adsorption performance for MB. For HNTs, the decolorization rate of MB is 41% after 20 min. After Fe, Ti, or Fe-Ti doping, their adsorption capacities are all improved mainly due to the increasing specific surface area resulting from ion exchange process under an acidic condition. And HNTs-Fe showed the highest adsorption capacity of MB, and reached the adsorption saturation after 20 min with the decolorization rate of 57%, mainly due to iron possessing perfect adsorption capacity [38, 39].

With comparison between the degradation performance and adsorption performance of different catalysts towards MB, it can be found that HNTs-Fe exhibits the highest MB adsorption capacity, while HNTs-Fe-Ti exhibits the highest Fenton-like catalytic degradation activity. The adsorption performance is benefit for improving the Fenton-like catalytic activity of the catalysts. However, it is not difficult to get the conclusion that the enhanced Fenton-like catalytic activity of HNTs-Fe-Ti mostly owes to Ti doping rather than its adsorption performance.

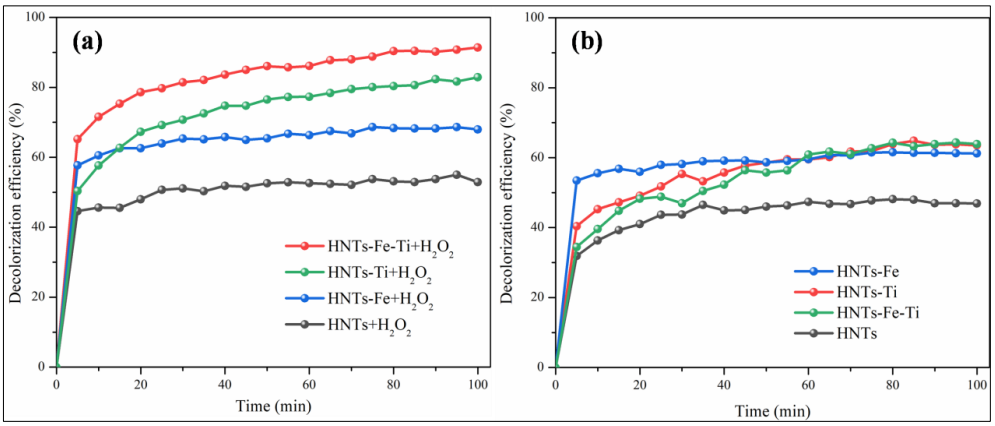

Figure 5. (a) Catalytic degradation performance and (b) adsorption performance of different catalysts (HNTs-Fe-Ti, HNTs-Ti, HNTs-Fe and HNTs) for MB

As Ti plays an important role in the degradation of MB for HNTs-Fe-Ti catalyst, the catalytic degradation performance of the prepared HNTs-Fe-Ti with different ratios of Fe and Ti were studied. The results are provided as shown in Figure 6a. When the ratios of Fe and Ti are 2:1 and 1:1, the MB decolorization rates of HNTs-Fe-Ti are 74 and 76% after 100 min, respectively. And the ratio of Fe and Ti reaches 1:5, the MB decolorization rate of HNTs-Fe-Ti increases to 91%. It shows that the Fenton-like degradation performance of the catalyst improves with the increasing content of Ti. However, the MB decolorization rate of HNTs-Fe-Ti has no obvious enhancement with further increasing content of Ti (the ratio of Fe and Ti is 1:10). As the result shows that the Fenton-like catalytic performance of HNTs-Fe-Ti with the ratio of 1:5 is optimal, the ratio of 1:5 is used in the following HNTs-Fe-Ti catalyst. Figure 6b shows the absorption spectra of MB solution taken at different reaction time, which demonstrates the Fenton-like catalytic efficiency of the HNTs-Fe-Ti catalyst explicitly. It can be seen the decolorization of MB aqueous solution has been almost accomplished after 100 min Fenton-like reaction.

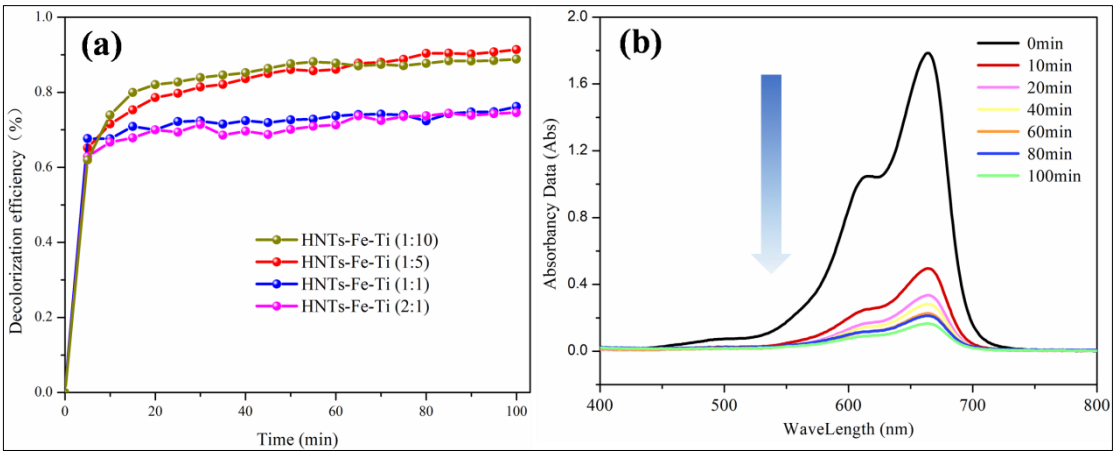

Figure 6. (a) Degradation performance of HNTs-Fe-Ti with various Fe and Ti ratios, (b) absorption spectra variance of MB solution taken at different reaction time for HNTs-Fe-Ti (1:5)

The decolorization of MB aqueous solution was carried out at different initial *p*H of the solution ranging from 3 to 11. And the effect of *p*H on degree of decolorization is presented in Figure 7a. The result shows that the degree of decolorization increases with the raised *p*H. At a lower *p*H of 3, the decolorization rate is 49.9%, while it could reach 89.8% at a higher *p*H of 11. The reason is that the

catalyst surface becomes negatively charged at higher *p*H, and adsorption rate of MB (positive charge) is becoming fast on the catalyst surface which is benefit for the decolourization reaction. Though the decolorization rate has decreased in a certain degree under acid condition, the HNTs-Fe-Ti catalyst still keeps good Fenton-like catalytic efficiency. Unlike other catalytic system the *p*H variance has a significant effect on Fenton-like catalytic efficiency [22, 40, 41]. As a consequence of it, the HNTs-Fe-Ti catalyst could be used in a variety of *p*H values. On the other hand, Figure 7b shows the recyclability of the HNTs-Fe-Ti catalyst for 5 cycles. The degradation performance for HNTs-Fe-Ti maintains at a decent level, MB decolourization rate could keep 80% after 5 times. It indicates the HNTs-Fe-Ti catalyst exhibits good recyclability for recovery and reuse. The higher reusability of the catalyst could be mainly related to the strong metal-support interaction between metal ions and HNTs which have excellent electrostatic adsorption ability for metal cations [35, 36].

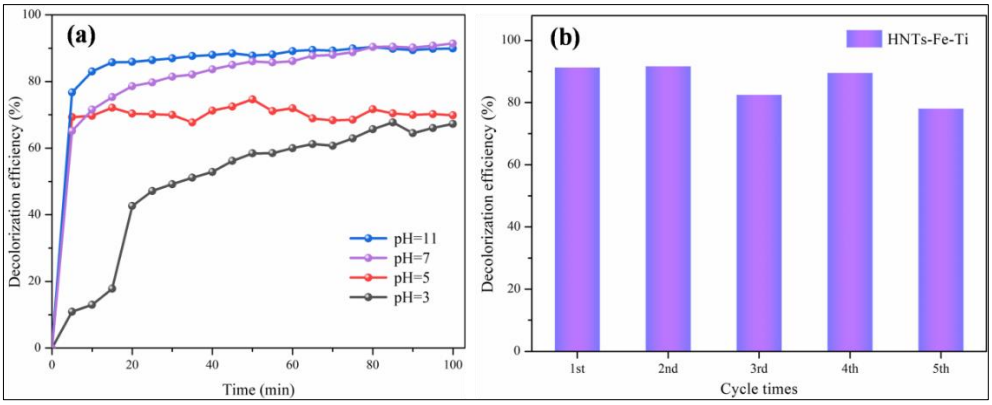

Figure 7. (a) Degradation efficiency of MB in various *p*H conditions, (b) test of catalytic cycle performance of HNTs-Fe-Ti catalyst

3.3. Fenton-like degradation mechanism of the HNTs-Fe-Ti catalyst

According to the catalytic degradation experiment, titanium ion plays important role in enhancing the Fenton-like degradation performance of the catalyst. In order to verify the valence state conversion mechanism of Ti in the catalytic degradation, the effect of catalytic degradation of HNTs-Fe-Ti and HNTs-Ti catalysts with and without KBH_4 reduction treatment were compared, respectively. On the other hand, $TiOSO_4$ and P25 with and without KBH_4 treatment were also used to further study the valence state conversion mechanism of Ti for Fenton-like reaction. The results are shown in Table 1. Obviously, the Fenton-like degradation performances of HNTs-Fe-Ti and HNTs-Ti catalysts are significantly improved after KBH_4 reduction. The decolorization rate of HNTs-Fe-Ti increases from 42 to 91%, while the decolorization rate of HNTs-Ti increases from 40 to 83%. Both of them with KBH_4 treatment have a superior Fenton-like degradation performance. Interestingly, the decolorization rates of the catalyst obtained from $TiOSO_4$ with KBH_4 treatment also show remarkable improvement (from 44% to 89%). However, the degradation rate of P25 has no obvious difference before and after KBH_4 treatment. It is mainly because P25 has a very stable lattice structure and Ti^{4+} is difficult to reduce into Ti^{3+}. And for $TiOSO_4$, reduction reaction is easy to happen. Hence, the degradation performance of P25 was limited. The results indicate that the valence state conversion maybe exists in the Fenton-like reaction of the HNTs-Fe-Ti and it plays important role in enhancing the Fenton-like degradation performance.

Table 1. Comparison of degradation performance of various catalysts with and without KBH_4 treatment

Catalyst	Decolorization rate at 100 min (without KHB_4)	Decolorization rate at 100 min (with KHB_4)
HNTs-Fe-Ti	42%	91%

HNTs-Ti	40%	83%
$TiOSO_4$	44%	89%
P25	11%	19%

To further confirm the existence of Ti^{3+} and demonstrate the valence state conversion of Ti, the surface chemical compositions and valence of HNTs-Fe-Ti and $TiOSO_4$ (treated with KBH_4) were investigated by X-ray photoelectron spectroscopy as shown in Figure 8a-c. The survey scan of HNTs-Fe-Ti (Figure 8a) exhibits O 1s, C 1s, Ti 2p and Fe 2p peaks indicating the successful Ti and Fe doping of HNTs. In addition, the Ti and Fe content on the surface of HNTs-Fe-Ti could be also observed from XPS results. The mass percentage of Ti and Fe are 2.89% and 1.04%, respectively. Figure 8b, c shows the Ti 2p high-resolution and curve fitting spectra of HNTs-Fe-Ti and $TiOSO_4$ (treated with KBH_4). For HNTs-Fe-Ti, the peaks at binding energies of 458.8 and 464.6 eV are typical features of Ti^{4+}, while the binding energies at 458.3 and 463.5 eV attribute to Ti^{3+} [42,43]. Besides, the area ratio of Ti^{4+} to Ti^{3+} is 25:7. Both of them indicate partial Ti^{4+} has been reduced into Ti^{3+}. As a comparison, $TiOSO_4$ (treated with KBH_4) sample also exhibits same typical peaks of Ti^{3+} and Ti^{4+}. The results from Figure 8b,c confirm the presence of Ti^{3+} enabling the valence state conversion between Ti^{3+} and Ti^{4+}. On the other hand, the digital photos of KBH_4 treated process of $TiOSO_4$ and P25 (Figure 8d) were recorded displaying an interesting color change. Dissolved $TiOSO_4$ solution is clear and transparent. But after adding KBH_4, a dark blue precipitate was formed in solution immediately. Because of the reduction of KBH_4, free Ti^{4+} in solution was easy to be reduced into Ti^{3+}. And Ti^{3+} tends to precipitate due to a changed *p*H. Then the dark blue precipitate turned into a white precipitate slowly, and became all white after 80 h. For comparison, P25 with stable lattice structure was treated with same process, and no color change could be observed. The results further verify the presence of Ti^{3+} for HNTs-Fe-Ti.

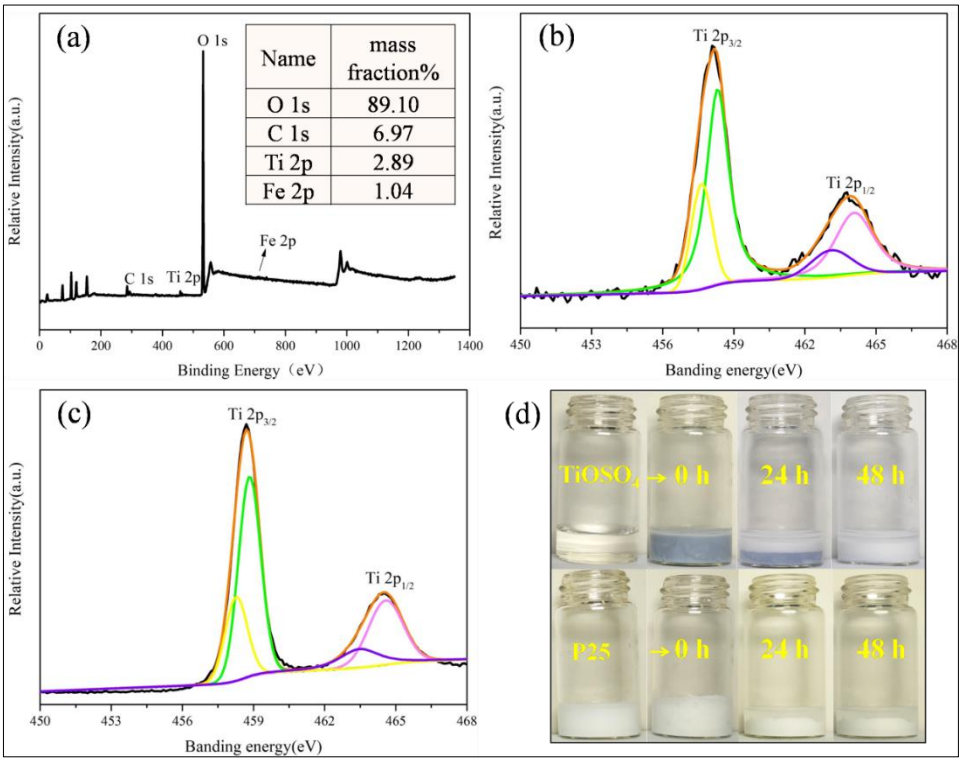

Figure 8. The XPS spectra of catalyst samples: (a) the survey scan of HNTs-Fe-Ti, Ti 2p region of (b) HNTs-Fe-Ti and (c) $TiOSO_4$ with KBH_4; (d) the digital photos of KBH_4 treated process of $TiOSO_4$ and P25

As the hydroxyl radical (•OH) is vital to destroy organic for Fenton-like reaction, the existence of •OH radicals was detected by DMPO-EPR spin-trapping which •OH determined by methanol as the

capture agent. The result is shown in Figure 9a, and four characteristic peaks of adducts with a typical intensity ratio of 1:2:2:1 were distinctively detected which are attributed to •OH [44]. It indicates •OH could produce during the Fenton-like reaction of HNTs-Fe-Ti catalyst. Besides, the effect of •OH capturing agent on the decolorization rate of HNTs-Fe-Ti catalyst was also discussed in Figure 9b which methanol (MeOH) was added as •OH trapping agent [45]. The results show an inhibitory effect could be observed when adding methanol, indicating that •OH plays an important role in the catalytic degradation reaction.

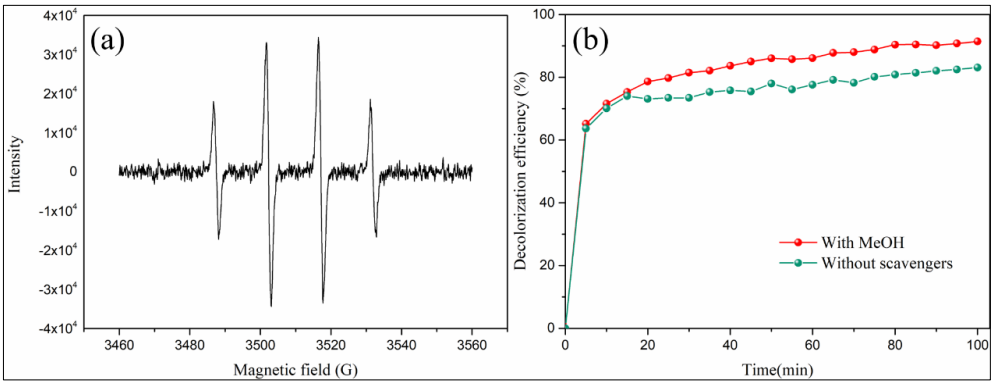

Figure 9. (a) EPR spectra of HNTs-Fe-Ti, (b) Effect of methanol on decolorization rate of HNTs-Fe-Ti catalyst

Fenton reagent can activate H_2O_2 by Fe^{2+} to produce hydroxyl radical. •OH is the main driving force for Fenton degradation of pollutants, which can attack a wide variety of organic compounds [46]. At present, the mechanism of Fenton reaction is described from equation 2 to 9.

$$H_2O_2+Fe^{2+}\rightarrow \bullet OH+Fe^{3+}+OH^- \quad (2)$$
$$Fe^{2+}+\bullet OH\rightarrow Fe^{3+}+OH^- \quad (3)$$
$$H_2O_2+Fe^{3+}\rightarrow Fe\text{-}OOH^{2+}+H^+ \cdot \quad (4)$$
$$H_2O_2+\bullet OH\rightarrow H_2O+HOO\bullet \cdot \quad (5)$$
$$Fe\text{-}OOH^{2+}\rightarrow HOO\bullet+Fe^{2+} \cdot \quad (6)$$
$$HO_2\bullet+Fe^{2+}+H^+\rightarrow Fe^{3+}+H_2O_2 \cdot \quad (7)$$
$$HO_2\bullet+Fe^{3+}\rightarrow Fe^{2+}+H_2O \quad (8)$$
$$RH+HO\bullet\rightarrow R\bullet+H_2O \quad (9)$$

Based on the above experimental results and according to pertinent literatures, a possible Fenton-like catalytic reaction mechanism of HNTs-Fe-Ti is proposed. First, the degradation of MB begins with surface adsorption of MB onto HNTs-Fe-Ti catalyst through microporous structures of HNTs. Then, the decolorization could be initiated by the •OH radicals which produced in Fenton-like reaction [47].

Here, the role of Ti is similar to the Fenton-like reaction mechanism of Fe, and the proposed mechanism is described in equation 10 to 18. In this process, Ti^{3+} loses electrons to become Ti^{4+}, then the electrons are captured by H_2O_2 to produce •OH. At the same time, Fe^0 interacts with H_2O_2 to form Fe^{2+}, Fe^{3+} and •OH which can be shown in equation 19 to 20 [48]. During the whole degradation process, •OH is dominant and produced •OH active species can attack the pollutants causing further degradation of MB.

$$Ti^{4+}+[H]\rightarrow Ti^{3+} \quad (10)$$
$$H_2O_2+Ti^{3+}\rightarrow \bullet OH+Ti^{4+}+OH^- \quad (11)$$
$$Ti^{3+}+\bullet OH\rightarrow Ti^{4+}+OH^- \quad (12)$$
$$H_2O_2+Ti^{4+}\rightarrow Ti\text{-}OOH^{3+}+H^+ \quad (13)$$
$$H_2O_2+\bullet OH\rightarrow H_2O+HOO\bullet \quad (14)$$
$$Ti\text{-}OOH^{3+}\rightarrow HOO\bullet+Ti^{3+} \quad (15)$$

$HO_2\bullet + Ti^{3+} + H^+ \rightarrow Ti^{4+} + H_2O_2$ (16)
$HO_2\bullet + Ti^{4+} \rightarrow Ti^{3+} + H_2O$ (17)
$RH + HO\bullet \rightarrow R\bullet + H_2O$ (18)
$Fe^0 + H_2O_2 \rightarrow Fe^{2+} + 2HO^-$ (19)
$Fe^{2+} + H_2O_2 \rightarrow Fe^{3+} + HO^- + HO\bullet$ (20)

4. Conclusions

In this paper, titanium-iron ion doped halloysite nanotubes have been developed as Fenton-like catalyst. Iron/titanium ions were successfully trace-doped into HNTs via simple ion-exchange reaction. The prepared catalyst exhibits enhanced Fenton-like catalytic performance in the presence of Ti^{3+}/Ti^{4+}. The results indicate that the excellent degradation ability mainly owes to the valence state transformation of titanium and the good adsorption ability of HNTs. And the important role of Ti on Fenton-like degradation reaction was demonstrated. This study designed a new type of catalyst and discovered the role of Ti^{3+}/Ti^{4+} valence state conversion mechanism in the catalytic degradation process. It will provide new ideas for the development of high-efficiency and more eco-friendly Ti-based Fenton-like catalysts.

Acknowledgments: The study received funding from the National Natural Science Foundation of China (21908251), Hunan Provincial Natural Science Foundation of China (2020JJ5962, 2020JJ2058), Hunan high-level talent gathering project-innovative talents (2019RS1061), PhD research startup foundation of Central South University of Forestry and Technology (104-0456), Scientific research project of Hunan Education Department (19A505).

References

1. KHATRI, A., PEERZADA, M.H., MOHSIN, M., WHITEC, M., A review on developments in dyeing cotton fabrics with reactive dyes for reducing effluent pollution, *J. Clean. Prod.*, **87**, 2015, 50-57. https://doi.org/10.1016/j.jclepro.2014.09.017
2. NALLATHAMBI, A., VENKATESHWARAPURAM RENGASWAMI, G.D., Industrial scale salt-free reactive dyeing of cationized cotton fabric with different reactive dye chemistry, *Carbohyd. Polym.*, **174**, 2017, 137-145. https://doi.org/10.1016/j.carbpol.2017.06.045
3.GUPTA, V.K., ALI, I., SALEH, T.A., NAYAKA, A., AGARWAL, S., Chemical treatment technologies for waste-water recycling-an overview, *RSC. Adv.*, **2**(16), 2012, 6380-6388. https://doi.org/10.1039/c2ra20340e
4. MINCU, M., MARCUS, M.I., MITIU, M.A., RAISCHI, N.S., Increasing the Efficiency of Pollutants Removal from Municipal Wastewater Using Biological Filters, *Rev. Chim.*, **69**(12), 2018, 3553-3556. https://doi.org/10.37358/RC.18.12.6790
5. LIU, M., ZHU, X., WEI, Y., ZHOU, H., LIU, R., HU, J., LIU, G., FAN, X., A novel hollowed‑out Si microsphere encapsulated by graphene oxide: a strong and reusable absorbent, *J. Porous. Mat.*, **27**, 2020, 979-987. https://doi.org/10.1007/s10934-020-00877-1
6. ISHPAL, PANWAR, O.S., KUMAR, M., KUMAR, S., X-ray photoelectron spectroscopic study of nitrogen incorporated amorphous carbon films embedded with nanoparticles, *Appl. Surf. Sci.*, **256**(24), 2010, 7371-7376. https://doi.org/10.1016/j.apsusc.2010.05.075
7. ORBECI, C., PASCU, L., MODROGAN, C., Degradation of Organic Compounds from Industrial Pharmaceutical Effluent Through Advanced Oxidation Processes, *Rev. Chim.*, **66**(4), 2015, 482-486. https://doi.org/10.37358/Rev.Chim.1949
8. COLLIVIGNARELLI, M.C., ABBA, A., CARNEVALE MIINO, M., DAMIANIET, S., Treatments for color removal from wastewater: State of the art, *J. Environ. Manage.*, **236**, 2019, 727-745. https://doi.org/10.1016/j.jenvman.2018.11.094
9. SIRES, I., BRILLAS, E., OTURAN, M.A., RODRIGO, M.A., PANIZZA, M., Electrochemical advanced oxidation processes: today and tomorrow, A review, *Environ. Sci. Pollut. R.,* **21**(14), 2014, 8336-8367. https://doi.org/10.1007/s11356-014-2783-1

10. JIMÉNEZ, S., ANDREOZZI, M., MICÓ, M.M., ÁLVAREZA, M.G., CONTRERAS, S., Produced water treatment by advanced oxidation processes, *Sci. Total. Environ.*, **666**, 2019, 12-21. https://doi.org/10.1016/j.scitotenv.2019.02.128
11. RIZZO, L., MALATO, S., ANTAKYALI, D., BERETSOU, V.G., ĐOLIĆ, M.B., GERNJAK, W., HEATH, E., IVANCEV-TUMBAS, I., KARAOLIA, P., LADO RIBEIRO, A.R., MASCOLO, G., MCARDELL, C., SCHAAR, H., SILVA, A.M.T., Fatta-Kassinos, D., Consolidated vs new advanced treatment methods for the removal of contaminants of emerging concern from urban wastewater, *Sci. Total. Environ.*, **655**, 2018, 986-1008. https://doi.org/10.1016/j.scitotenv.2018.11.265
12. MIKLOS, D.B., REMY, C., JEKEL, M., LINDEN, K.G., DREWES, J.E., HÜBNER, U., Evaluation of advanced oxidation processes for water and wastewater treatment-A critical review, *Water Res.*, **139**, 2018, 118-131. https://doi.org/10.1016/j.watres.2018.03.042
13. SHI, X., TIAN, A., YOU, J., YANG, H., WANG, Y., XUE, X., Degradation of organic dyes by a new heterogeneous Fenton reagent-Fe_2GeS_4 nanoparticle, *J. Hazard. Mater.*, **353**, 2018, 182-189. https://doi.org/10.1016/j.jhazmat.2018.04.018
14. CHEN, H., MOTUZAS, J., MARTENS, W., DINIZ DA COSTA, J.C., Degradation of azo dye orange II under dark ambient conditions by calcium strontium copper perovskite, *Appl. Catal. B-Environ.*, **221**, 2017, 691-700. https://doi.org/10.1016/j.apcatb.2017.09.056
15. MINELLA, M., MARCHETTI, G., DE LAURENTIIS, E., MALANDRINO, M., MAURINO, V., MINERO, C., VIONEA, D., HANNA, K., Photo-Fenton oxidation of phenol with magnetite as iron source, *Appl. Catal. B-Environ.*, **154-155**, 2014.102-109. https://doi.org/10.1016/j.apcatb.2014.02.006
16. KIAMERTH, N., MALATO, S., AGUEERA, A., FERNÁNDEZ-ALBAB, A., Photo-Fenton and modified photo-Fenton at neutral pH for the treatment of emerging contaminants in wastewater treatment plant effluents: A comparison, *Water Res.*, **47**(2), 2013, 833-840. https://doi.org/10.1016/j.watres.2012.11.008
17. GUO, L., CHEN, F., FAN, X., CAI, W., ZHANG, J., S-doped α-Fe_2O_3 as a highly active heterogeneous Fenton-like catalyst towards the degradation of acid orange 7 and phenol, *Appl. Catal. B-Environ.*, **96**(1-2), 2010, 162-168. https://doi.org/10.1016/j.apcatb.2010.02.015
18. DRAGOI, M., MOANŢĂ, A., TIGAE, C., Removal of Some Triphenylmethane Dyes from Aqueous Solutions by Fenton Reagent. I, *Rev. Chim*., **66**(9), 2015, 1273-1277. https://doi.org/10.37358/Rev.Chim.1949
19. ZHANG, J., ZHUANG, J., GAO, L., ZHANG, Y., GU, N., FENG, J., YANG, D., ZHU, J., YAN, X., Decomposing phenol by the hidden talent of ferromagnetic nanoparticles, *Chemosphere*, **73**(9), 2008, 1524-1528. https://doi.org/10.1016/j.chemosphere.2008.05.050
20. LU, B., LIU, G., LIU, M., ZHU, X., LIU, H., XU, B., CHANG, S., LIU, Y., HU, J., Facile preparation of nano-Fe_3O_4/micro-carbon fiber from waste paper as self-propulsive solar-Fenton catalyst with excellent degradation performance and reusability, *Desalin. Water Treat.*, **191**, 2020, 300-309. https://doi.org/10.5004/dwt.2020.25714
21. LI, Y., ZHANG, F., Catalytic oxidation of Methyl Orange by an amorphous FeOOH catalyst developed from a high iron-containing fly ash, *Chem Eng J*, **158**(2), 2009, 148-153. https://doi.org/10.1016/j.cej.2009.12.021
22. PINTO, I.S.X., PACHECO, P.H.V.V., COELHO, J.V., LORENÇON, E., ARDISSON, J.D., FABRIS, J.D., SOUZA, P.P.D., KRAMBROCK, K.W.H., OLIVEIRA, L.C.A., Pereira, M.C., Nanostructured *δ*-FeOOH: An efficient Fenton-like catalyst for the oxidation of organics in water, *Appl. Catal. B-Environ.*, **119-120**, 2012, 175-182.https://doi.org/10.1016/j.apcatb.2012.02.026
23. ZOU, X., ZHOU, T., MAO, J., WU, X., Synergistic degradation of antibiotic sulfadiazine in a heterogeneous ultrasound-enhanced Fe^0/persulfate Fenton-like system, *Chem. Eng. J.*, **257**, 2014,36-44. https://doi.org/10.1016/j.cej.2014.07.048

24. PAN, Y., ZHOU, M., LI, X., XU, L., TANG, Z., LIU, M., Novel Fenton-like process (pre-magnetized Fe^0/H_2O_2) for efficient degradation of organic pollutants, *Sep. Purif. Technol.*, **169**, 2016, 83-92. https://doi.org/10.1016/j.seppur.2016.06.011
25. ZHANG, N., YI, Y., LIAN, J., FANG, Z., Effects of Ce doping on the Fenton-like reactivity of Cu-based catalyst to the fluconazole, *Chem. Eng. J.*, **395**, 2020, 124897-124907. https://doi.org/10.1016/j.cej.2020.124897
26. HAZARIKA, K.K., TALUKDAR, H., SUDARSANAM, P., BHARGAVA, S., BHARALI, P., Highly dispersed Mn_2O_3-Co_3O_4 nanostructures on carbon matrix as heterogeneous Fenton-like catalyst, *Appl. Organomet. Chem.*, **34**(4), 2020,1-13.https://doi.org/10.1002/aoc.5512
27. YAO, Y., CAI, Y., WU, G., WEI, F., LI, X., CHEN, H., WANG, S., Sulfate radicals induced from peroxymonosulfate by cobalt manganese oxides ($Co_xMn_{3-x}O_4$) for Fenton-Like reaction in water, *J. Hazard. Mater.*, **296**, 2015, 128-137. https://doi.org/10.1016/j.jhazmat.2015.04.014
28. YAO, Y., CHEN, H., CHAO, L., WEI, F., ZHANG, D., WU, G, CHEN, B, WANG, S., Fe, Co, Ni nanocrystals encapsulated in nitrogen-doped carbon nanotubes as Fenton-like catalysts for organic pollutant removal, *J. Hazard. Mater.*, **314**, 2016, 129-139. https://doi.org/10.1016/j.jhazmat.2016.03.089
29. LIANG, X., ZHONG, Y., HE, H., YUAN, P., ZHU, J., ZHU, S., ZHENG, J., The application of chromium substituted magnetite as heterogeneous Fenton catalyst for the degradation of aqueous cationic and anionic dyes, *Chem. Eng. J.*, **191**, 2012, 177-184.https://doi.org/10.1016/j.cej.2012.03.001
30. EGOROVA, K.S., ANANIKOV, V.P., Which metals are green for catalysis? Comparison of the toxicities of Ni, Cu, Fe, Pd, Pt, Rh, and Au salts, *Angew Chem. Int. Ed. Engl.*, **55**(40), 2016, 12150-12162. https://doi.org/10.1002/chin.201645197
31. MASAE, M., SIKONG, L., KONGSONG, P., PHOLTHAWON, C., PAWANWATCHARAKORN, N., ABDULLAH, M.M.A.B., SANDU, A.V., Super hydrophilicity and photocatalytic activity of potassium doped TiO_2 nanoparticulate films, *Rev. Chim.* **67**(9), 2016, 1884-1890. https://doi.org/10.37358/Rev.Chim.1949
32. CHEN, S., XIAO, Y., WANG, Y., HU, Z., ZHAO, H., XIE, W., A facile approach to prepare black TiO_2 with oxygen vacancy for enhancing photocatalytic activity, *Nanomaterials-Basel*, **8**(4), 2018, 245-261. https://doi.org/10.3390/nano8040245
33. DENG, A., ZHU, Y., GUO, X., ZHOU, L., JIANG, Q., Synthesis of various TiO_2 Micro-/Nano-Structures and their photocatalytic performance, *Materials*, **11**(6), 2018, 1-11. https://doi.org/10.3390/ma11060995
34.ZHAO, Z., TAN, H., ZHAO, H., LV, Y., ZHOU, L., SONG, Y., SUN, Z., Reduced TiO_2 rutile nanorods with well-defined facets and their visible-light photocatalytic activity, *Chem. Commun.*, **50**(21), 2014, 2755-2757. https://doi.org/10.1039/c3cc49182j
35. RIELA, S., MASSARO, M., CAVALLARO, G., COLLETTI, C., LAZZARA, G., MILIOTO, S., NOTO, R., Chemical modification of Halloysite nanotubes for controlled loading and release, *J. Mater. Chem. B.*, **6**(21), 2018, 3415-3433. https://doi.org/10.1039/C8TB00543E
36. ISMAIL, A.F., HASHEMIFARD, S.A., MATSUURA, T., Facilitated transport effect of Ag^+ ion exchanged halloysite nanotubes on the performance of polyetherimide mixed matrix membrane for gas separation, *J. Membrane. Sci.*, **379**(1-2), 2011, 378-385.https://doi.org/10.1016/j.memsci.2011.06.010
37.WANG, Q., WANG, Y., ZHAO, Y., ZHANG, B., NIU, Y., XIANG, X., CHEN, R., Fabricating roughened surfaces on halloysite nanotubes via alkali etching for deposition of high-efficiency Pt nanocatalysts, *Crystengcomm*, **17**, 2015, 3110-3116.https://doi.org/10.1039/c5ce00189g
38. REGUYAL, F., SARMAH, A.K., GAO, W., Synthesis of magnetic biochar from pine sawdust via oxidative hydrolysis of $FeCl_2$ for the removal sulfamethoxazole from aqueous solution, *J. Hazard. Mater.*, **321**, 2017,868-878. https://doi.org/10.1016/j.jhazmat.2016.10.006
39. ZHANG, P., O'CONNOR, D., WANG, Y., JIANG, L., XIA, T., WANG, L., TSANG, D.C.W., OK, Y.S., HOU, D., A green biochar/iron oxide composite for methylene blue removal, *J. Hazard. Mater.*, **384**, 2020, 12186-12194. https://doi.org/10.1016/j.jhazmat.2019.121286

40. JIANG, C., PANG, S., OUYANG, F., MA, J., JIANG, J., A new insight into Fenton and Fenton-like processes for water treatment, *J. Hazard. Mate.,* **174**(1-3), 2010, 813-817. https://doi.org/10.1016/j.jhazmat.2009.09.125
41. PANDA, N., SAHOO, H., MOHAPATRA, S., Decolourization of Methyl Orange using Fenton-like mesoporous Fe_2O_3-SiO_2 Composite, *J. Hazard. Mater.,* **185**(1), 2010, 359-365. https://doi.org/10.1016/j.jhazmat.2010.09.042
42. CHINH, V.D., BROGGI, A., DI PALMA, L., SCARSELLA, M., SPERANZA, G., VILARDI, G., THANG, P.N., XPS spectra analysis of Ti^{2+}, Ti^{3+} ions and dye photodegradation evaluation of titania-silica mixed oxide nanoparticles, *J. Electron. Mater.*, **47**, 2018, 2215-2224. https://doi.org/10.1007/s11664-017-6036-1
43. KANG, Q., CAO, J., ZHANG, Y., LIU, L., XU, H., YE, J., Reduced TiO_2 nanotube arrays for photoelectrochemical water splitting, *J. Mater. Chem. A.*, **18**, 2013, 5766-5774. https://doi.org/10.1039/c3ta10689f
44. SUN, Y., WANG, H., XING, Q., CUI, W., LI, J., WU, S., SUN, L., The pivotal effects of oxygen vacancy on Bi_2MoO_6: Promoted visible light photocatalytic activity and reaction mechanism, *Chinese J. Catal.*, **40**(5), 2019, 647-655. https://doi.org/10.1016/S1872-2067(19)63277-8
45. CHEN, J., ZHU, L., Catalytic degradation of Orange II by UV-Fenton with hydroxyl-Fe-pillared bentonite in water, *Chemosphere*, **65**(7), 2006, 1249-1255. https://doi.org/10.1016/j.chemosphere.2006.04.016
46. BOCZKAJ, G., FERNANDES, A., Wastewater treatment by means of advanced oxidation processes at basic pH conditions: A review, *Chem. Eng. J.*, **320**, 2017, 608-633. https://doi.org/10.1016/j.cej.2018.01.049
47. BARAKAT, M.A., KUMAR, R., BALKHYOUR, M.,TALEBA, M.A., Novel Al_2O_3/GO/halloysite nanotube composite for sequestration of anionic and cationic dyes, *RSC. Adv.*, **9**(24), 2019, 13916-13926. https://doi.org/10.1039/C9RA02246E
48. WU, Y., ZENG, S., WANG, F., MEGHARAJ, M., NAIDU, R., CHEN, Z., Heterogeneous Fenton-like oxidation of malachite green by iron-based nanoparticles synthesized by tea extract as a catalyst, *Sep. Purif. Technol.*, **154**, 2015, 161-167. https://doi.org/10.1016/j.seppur.2015.09.022

Manuscript received: 27.10.2020